4 Catalytic Activity of Ni SACs Towards Hydrogen Evolution Reaction

In this chapter, we discuss our work on investigating the catalytic activity of Ni SACs supported over various kinds of substrates like carbon-based (graphene and AlC), nitrides (h-BN and AlN) and oxides (BeO and MgO) (Ni@2D) towards hydrogen evolution reaction (HER). Here, we have considered various anchoring sites like top, bridge, hollow and defects and computed binding energy (E_b) to analyse stability of Ni-SACs. Further, we calculated the HER activity predictor i.e., about the differential Gibbs free energy of H-adsorption (ΔG_H), and plotted volcano-like structure which provides quantitative idea about the strength of H-adsorption. Then, we considered Volmer-Heyrovsky (VH) and Volmer-Tafel (VT) mechanism of HER and computed minimum energy path and activation energy (E_a) for the shortlisted systems based on E_b, ΔG_H. Our study found that Ni@AlN and Ni@h-BN with E_a values i.e., 0.12 eV and 0.21 eV, 0.28 eV and 0.26 eV via VT and VH mechanisms, are potential, eco-operational candidates to replace the existing high-cost Pt-based catalyst.

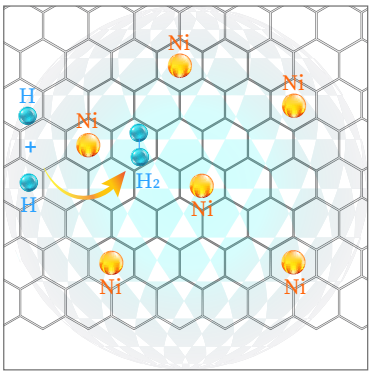

FIGURE 4.1: Graphical Abstract

4.1 Introduction

The hydrogen evolution reaction (HER) is subject of pervasive research as it is one of those crucial chemical processes that leads to generation of an ecologically-clean and sustainable energy source i.e., hydrogen (H_2)[1]. The versatility of H_2 makes its production a burning need at the moment due to its expediency (i) in fuel for vehicles and spacecrafts with zero-carbon footprint[2], (ii) in fuel cells to generate electricity[3], (iii) as a compact energy carrier due to its high energy density[4], (iv) as a feedstock for various important industrial chemical processes/conversion like in synthesis of ammonia (NH_3) from N_2[5], in CO_2 reduction to formic acid (HCOOH), hydrocarbons (C_nH_x), alcohols (C_nH_xOH) etc.[6], that sets H_2 an exemplar component in techno-chemical industries. Although, there are various chemical reactions which yield H_2 like water-gas shift reaction[7, 8], coal gasification[9], steam methane reforming[10] etc., either as a main product or by-product, but the HER has the edge among these reaction mainly due to (i) absence of carbon-containing compounds in the whole process of H_2 generation, as an effect improving the longevity of the catalyst used and (ii) decentralized production units deployment attainable at smaller scale reducing the requirements of large-unit setup and soothing the transportation issue[11, 12]. On the flip side, there are some significant issues in HER that require the time and efforts of researchers like, the existing catalyst are mainly comprised of Pt-based systems[13]. The noble-nature, big-ticket value and paucity of Pt, questions the long-term applicability of Pt-based catalysts[14]. Moreover, the inadequacy of Pt-catalyst to break H-OH bond in overall water splitting reaction degrades the efficiency of catalyst on repeated usage[15]. Thus, there is indeed an imperative need to unearth an impactful alternative of Pt as a catalyst for HER. Typically, transition-metals (TMs) based catalysts are attested to manifest first-rate catalytic activity for various chemical reaction attributed to their partially filled d-orbitals and adroitness of variable oxidation states[16]. For the same reason, TMs based catalyst are broadly investigated for HER too.

Although, investigation of catalyst for HER is broadly researched topic, but the emergence of new concepts in catalysis, updated synthesis/characterization techniques, modern reaction-probing technologies and advanced computational tools and methods creates fresh opportunities and possibilities to explore un-touched ways of designing a practically applicable catalyst. As the catalytic performance is known to be affected eminently by the catalyst particle size, the downsizing of

catalyst particle, from bulk to 2D to nanoclusters alters the electronic properties and also increase the specific area for the reactants, thereby amplifying the catalytic activity[17, 18]. This approach of downsizing the particle further headed to the atomic-scale, wherein the atomically dispersed atoms act as an active site known as single-atom catalysts (SACs)[19, 20]. The strikingly embellished catalytic activity of SACs is due to the introduction of quantum confinement effect at the atomistic-level leading to emergence of frontier orbitals that interact with reactants optimally thereby improving activity and selectivity of SACs[21]. Thus, in the past decade or so, the investigation of SACs for various prime chemical reactions are increased exponentially. Various SACs like TM SACs on defected graphene and h-BN sheet (TM= Fe, Co, Ni, Ru, Rh, Pd, Os, Ir, Pt)[22], Fe over graphene[23], Pt anchored Graphdiyne[24] and many more are explored both theoretically and experimentally for efficient HER[1, 25]. The catalytic behaviour of SACs is greatly affected by the support/substrate used to anchor the single-atoms. The interaction of single-atoms with the substrate not only stabilize the atoms but also alters the electronic structure of the adatoms, thereby affecting the electro-catalytic properties. Thus, in a way, the activity of the SACs could well presume to originate from the metal-support interaction[26]. Thus, it is of great significance to explore various kinds of supports for a particular SACs towards a particular reaction.

In this work, we examined structural-electronic properties, interaction of H-atom and finally the complete reaction mechanism of HER via two possible reaction mechanisms (i) Volmer-Heyrovsky (VH) and (ii) Volmer-Tafel (VT) mechanism[27], over Ni SACs supported over various class of 2D (Ni@2D) substrates like, carbon-based (graphene[28] and AlC[29]), nitrides (AlN[30, 31] and h-BN[32]) and oxides (BeO and MgO)[33]. The complete reaction and energy profiles are discussed later in the article. This research provides a thorough insight of HER over Ni SACs on class of substrates by a thorough insight into interaction mechanistic of H-atom with Ni@2D, analysis of HER activity predictors like differential Gibbs free energy of H-adsorption (ΔG_H), volcano plot analysis, investigation of complete reaction profile and computation of minimum energy path and activation energy. This research comprehensively articulates the fundamentals of HER, the principles governing the activity of HER catalyst and presents an exhaustive way in rational design of practicably eco-applicable SACs for HER.

4.2 Methodology

4.2.1 Total Energy Calculation

All the self-consistent total energy calculations were performed using Quantum ESPRESSO simulation package based on density functional theory (DFT)[34, 35]. Spin-polarization is considered for all the calculations as the considered systems involve TMs. We considered all-electron projected augmented wave (PAW) pseudopotentials to consider electron-ion interactions[36, 37]. To evaluate electronic exchange-correlation interactions, generalized gradient approximation (GGA) in the framework of Perdew–Burke–Ernzerhof (PBE) were used[38]. , The semi-empirical van der Waals corrections DFT-D3 proposed by Grimme et. al were employed to consider the long-range dispersion forces[39]. To avoid interaction between two periodic images a vacuum of 18 Å was provided in **z**-direction . The kinetic energy cut-off of 100 Ry was chosen to be for the plane-wave basis set. The convergence threshold set to 1.0×10^{-6} eV without applying any symmetry constraints was considered for geometry optimization. The Marzari-Vanderbilt smearing method with a finite temperature width of 0.02 Ry was adopted[40]. Supercells consisting of $4 \times 4 \times 1$ unit cell of of considered 2D systems were used and the Brillouin zones were sampled using a Monkhorst–Pack scheme with $8 \times 8 \times 1$ **k**-points grid[41].

4.2.2 Minimum Energy Path and Activation Energy Computation

The computation of complete reaction profiles and activation barrier of HER were investigated using the climbing image nudged elastic band (CI-NEB) method. (implemented in the Quantum ESPRESSO)[42, 43]. The activation energy barrier (E_a) for rate determining step was calculated as

$$E_a = E_{TS} - E_{IS/IM} ...(1)$$

Where E_{TS} and $E_{IS/IM}$ are the energies of transition state, initial/intermediate state (depend on the nature of reaction). To prepare all visual depictions of the structures under investigation XCrySDen visualization package was used [44].

4.3 Results and Discussion

4.3.1 Structural Analysis

As discussed in introduction, the substrate plays significant role in anchoring and stabilizing SACs and also it alters the electronic structure which results in enhanced catalytic activity of SACs. Thus, here we aimed to explore variety of 2D substrates XY to anchor the Ni SACs, where, X, Y being C, C; Al, C; Al, N; B, N; Be, O; Mg, O for graphene, AlC, AlN, h-BN, BeO and MgO, respectively as shown in Fig.4.2 (a-f). For all these substrates, there are various possible anchoring sites for Ni SACs like X-top, Y-top, bridge, hollow, X-vacancy and Y-vacancy. In such a way, there are total 34 anchoring sites for Ni-atoms. Having large number of

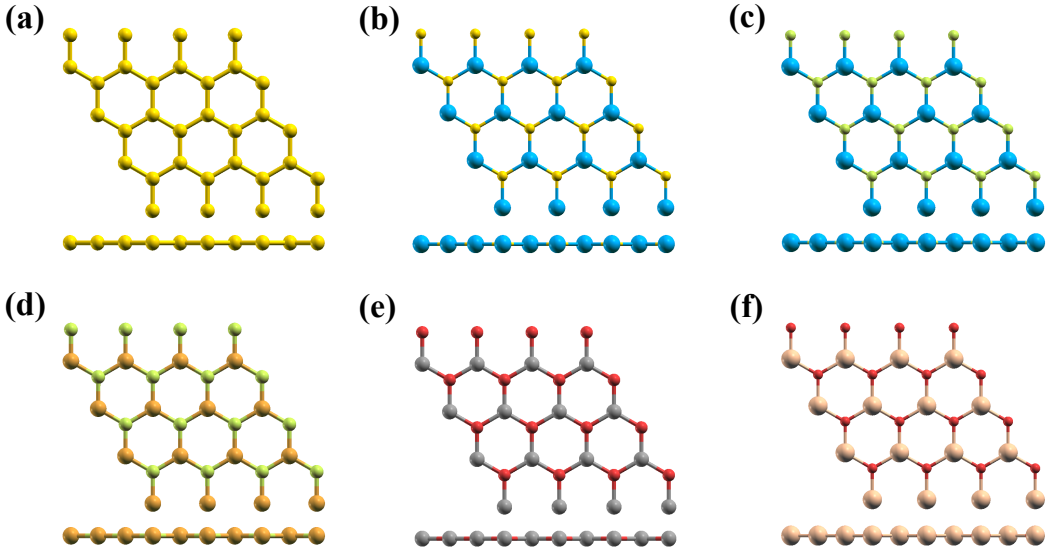

FIGURE 4.2: Optimized geometry of 4 × 4 × 1 supercell of (a) Graphene, (b) AlC, (c) AlN, (d) h-BN (e) BeO and (f) MgO. Yellow, blue, light green, orange, gray, red and cream sphere represent C, Al, N, B, Be, O and Mg atom, respectively.

sites, we first applied screener on the stability of Ni@2D as the stability of SACs is crucial to perform any catalytic process over it. The most basic parameter to judge the stability is the interaction of SACs with the substrate. The stronger interaction will lead to stable of single-atoms. The binding energy (E_b) calculation describes the interaction of single-atoms with substrate quantitatively and is calculated using.

$$E_b(Ni) = E_{Ni@2D} - E_{2D} - E_{Ni} ...(2)$$

TABLE 4.1: The binding energy (E_b), differential Gibbs free energy of H-adsorption (ΔG_H), overpotential (η) and activation energy E_a via VH and VT mechanism for the selected configurations of Ni@2D.

System	Site	E_b(Ni) (eV)	ΔG_H (eV)	η (mV)	E_a (eV) (VH)	E_a (eV) (VT)
Graphene	Hollow	-3.55	-1.57	1570	-	-
	C_vac	-6.49	-0.24	240	0.78	0.71
AlC	Hollow	-3.32	0.49	490	1.64	1.21
	Al_vac	-5.01	-0.18	180	0.63	0.56
	C_vac	-4.38	-0.36	360	0.97	0.76
AlN	Hollow	-3.28	-1.57	1570	-	-
	Al_vac	-6.89	-0.06	60	0.21	0.12
	N_vac	-3.91	-0.76	760	-	-
h_BN	Hollow	-3.05	-0.69	690	-	-
	B_vac	-7.36	-0.09	90	0.36	0.28
	N_vac	-4.1	-0.38	380	0.48	0.4
BeO	Hollow	-3.2	-1.07	1070	-	-
	Be_vac	-4.95	-0.21	210	1.12	0.84
	O_vac	-4.29	-0.77	770	-	-
MgO	Hollow	-3.06	-1.4	1400	-	-
	Mg_vac	-4.86	-0.33	330	0.86	0.69
	O_vac	-4.78	-0.21	210	1.23	1.02

where, $E_{Ni@2D}$, E_{2D} and E_{Ni} are the total energy of Ni@2D, energy of 2D substrate and energy of isolated Ni-atom, respectively.

We calculated $E_b(Ni)$ for all the sites over considered substrates and considering the significance of stability of SACs, the further calculations have been performed wherein the E_b(Ni)< -3.00 eV and the exact values for those configurations are presented in Table A.2. As it can be observed from the table, the hollow and vacancy sites are more favourable while the bridge/top sites are not preferred for anchoring of Ni-atoms. Thus, out of 34 configurations, 17 configurations were having E_b value <-3.00 eV and those are considered for H adsorption and further analysis.

4.3.2 Reaction Mechanism and H-Adsorption

Electrocatalytic HER is basically a cathodic half reaction of overall water-splitting reaction[45, 46] and it proceed in two elementary reaction process, first being the discharge reaction as $H^+ + e^- \rightarrow H_{ads}$, this step is known as Volmer step. The Volmer step is followed by either Heyrovsky step i.e., electrochemical desorption as

$H^+ + e^- + H_{ads} \rightarrow H_2^{(g)}$ or Tafel step i.e., combination desorption as $H_{ads} + H_{ads} \rightarrow H_2^{(g)}$[27]. The overall performance of the catalyst towards HER heavily depends on how well the catalyst perform the Volmer step i.e., how well the H-adsorption takes place over the surface of the catalyst. According to the Sabatier principle, the interaction of H-atom shouldn't be too strong, which poses difficulty in releasing the product or the interaction shouldn't be too weak so that the reaction process does not initiate on the surface of catalyst[47, 48]. The interaction of H-atom should be optimum in order to have an efficient reaction process. Thus, it is of foremost prominence to inspect the H-interaction with Ni SACs. Therefore, we proceed with the adsorption of H-atom on selected configurations of Ni SACs. The adsorption energy (E_{ads}) of H-atom over Ni SACs is calculated as

$$E_{ads}(H) = E_{H+Ni@2D} - E_{Ni@2D} - \frac{1}{2}E_{H_2} ...(3)$$

where, $E_{H+Ni@2D}$, $E_{Ni@2D}$ and E_{H_2} are the total energy of H adsorbed Ni@2D, energy of Ni@2D and energy of H_2 molecule, respectively.

The E_{ads} is found to vary from 0.25 eV to -1.81 eV over the considered candidates. Although the E_{ads} gives an idea about the strength of the interaction between H-atom and Ni SACs, but it does not provide insight into whether the interaction is optimum or not.

The differential Gibbs free energy of H-adsorption (ΔG_H) is an accurate quantita-

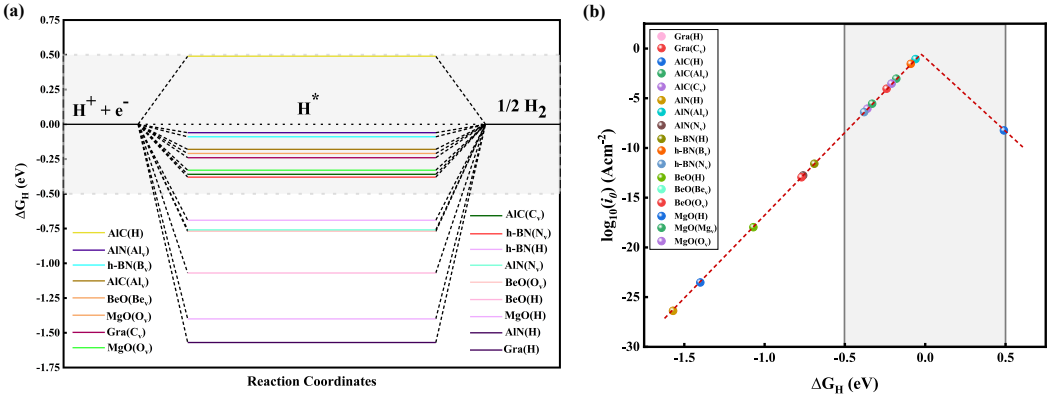

FIGURE 4.3: (a) differential Gibbs free energy (ΔG_H) of hydrogen adsorption over Ni@2D on various sites/substrates. (b) Volcano plot between exchange current density and ΔG_H for Ni@2D.

tive parameter that gives an indication about the optimum strength of interaction. Accordingly, the ΔG_H value closer to zero signatures the optimum H-interaction resulting in superior activity towards HER, while more negative (positive) value of

ΔG_H results in stronger (weaker) interaction between H-atom and catalyst, curtailing the activity of catalyst substantially[49, 50].The ΔG_H value is calculated using

$$\Delta G = E_{ads}(H) + \Delta E_{ZPE} - T\Delta S + eU + k_B T(\ln\ 10) * pH ...(4)$$

where $E_{ads}(H)$ is the adsorption energy of H-atom over Ni@2D, $\Delta E_{ZPE} - T\Delta S$ =0.24 eV (free energy correction term), electrode potential U and pH are considered as 0[51, 52].

Fig.4.3 (a) shows the plot of ΔG_H with reaction coordinates of H adsorption for all considered configuration. The ΔG_H value ranges between -1.57 eV to 0.49 eV (Table A.2) for all considered configuration of Ni@2D. As discussed above about the optimum value of ΔG_H is near about 0 eV, so we again applied a screener in our study. Since, the value ranges from -1.57 eV to 0.49 eV, we considered those configurations of Ni@2D in which the $|\Delta G_H| \leq 0.50$ eV as shown by the shaded region in the plot (Fig4.3 (a-b)). Out of 17 configurations of Ni@2D, 10 were falling in the selected region with best ΔG_H value for Ni@AlN (at Al-vacancy) and Ni@h-BN (at B-vacancy) of -0.06 eV and -0.09 eV, respectively. Moreover, according to the classic 'volcano' theory, the volcano plot analysis between exchange current density (i_0) and ΔG_H serves as prime indicator for the HER activity[53]. The i_0 for various configurations is calculated as

$$i_0 = -ek_0 \frac{1}{1+\exp\left(-\frac{\Delta G_H}{k_B T}\right)} \text{ for } \Delta G_H < 0 ...(5)$$

$$i_0 = -ek_0 \frac{1}{1+\exp\left(\frac{\Delta G_H}{k_B T}\right)} \text{ for } \Delta G_H > 0 ...(6)$$

Here, the rate constant $k_0 = 1 s^{-1} site^{-1}$ according to Nørskov's approximation and e is taken as unity[53–55].

In the volcano plot as shown in Fig.4.3 (b), the optimum H-binding and thus the maximum HER activity is to be found at the top of the plot with $\Delta G_H \approx 0$ eV. In alignment with the above results, Ni@AlN and Ni@h-BN occupies the top of the plot, assenting the prediction of superior HER activity of the above systems. The absolute value of ΔG_H, i.e., $|\Delta G_H|$ is regarded as theoretical overpotential η[56, 57], is presented in Table A.2 with the lowest η value found is 60 mV and 90 mV for the above specified two systems.

4.3.3 Minimum Energy Path and Activation Energy Calculations

After examining the H-adsorption, ΔG_H and volcano plot, we screened the 10 configurations of Ni@2D which has ΔG_H value in the range -0.5 eV to 0.5 eV to study the complete reaction profile of HER, the minimum energy path and activation energy calculations. We considered Volmer-Heyrovsky (VH) and Volmer-Tafel (VT) mechanisms to study the HER activity of Ni@2D.

4.3.3.1 VH Mechanism

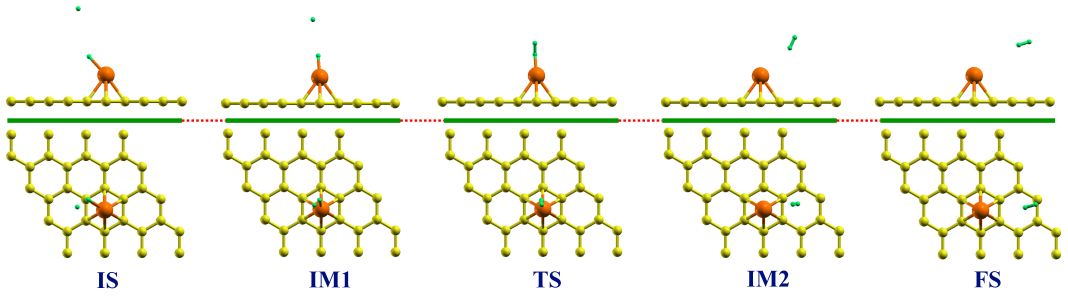

FIGURE 4.4: Generalized reaction profile of HER via VH mechanism over Ni@2D.

The complete reaction profile of HER via VH mechanism is presented in Fig.4.4. In VH mechanism, the initial state (IS) is comprised of a pre-adsorbed H-atom at Ni@2D exposed to another H, reacting to form a complex like *HH (* denotes an adsorption site) as a transition state (TS) via intermediate state (IM). The *HH complex the leaves to form $H_2^{(g)}$ in the final state (FS) of the reaction. The energy profile of the corresponding HER over Ni@2D is depicted in Fig.4.5 (a).

The activation energy (E_a) values of HER via VH mechanism over considered Ni@2D configurations varies from 0.21 eV to 1.64 eV, the lowest is for Ni@AlN at Al-vacancy. There are other configurations of Ni@2D like Ni@h-BN exhibits E_a of 0.36 eV (B-vacancy) and 0.48 eV (N-vacancy), Ni@AlC has E_a of 0.63 eV (at Al-vacancy) could be considered to showcase relatively good catalytic activity with these moderate reaction barrier values.

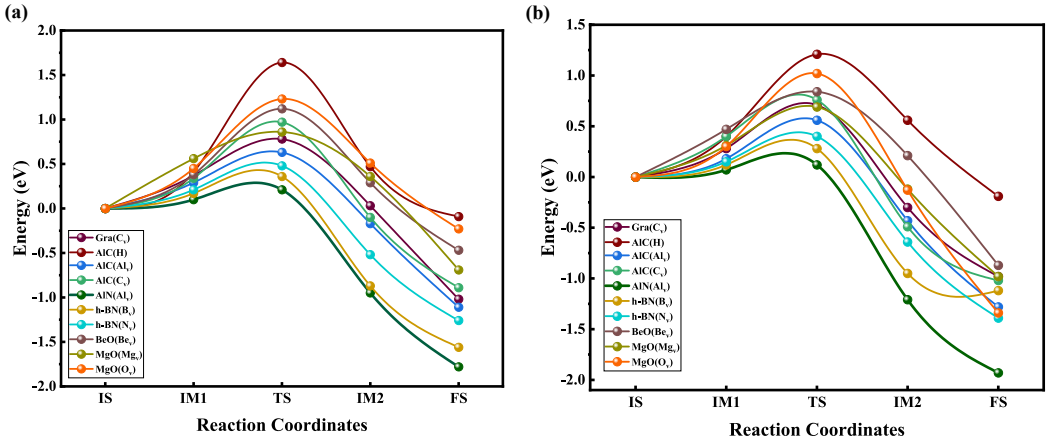

FIGURE 4.5: Complete energy profile of HER via (a) VH mechanism and (b) VT mechanism over selected configurations of Ni@2D.

4.3.3.2 VT Mechanism

Further, the complete reaction profile of HER via VT mechanism is examined and sketched in Fig.4.6. In VT mechanism, the IS formed as two co-adsorbed H-atoms, reacts on the active site to form a triangular H-Ni-H complex as TS, then dissociating into $H_2^{(g)}$ as a product. The minimum energy path of HER via VT mechanism is shown in Fig.4.5 (b). The E_a values via VT mechanism over Ni@2D systems

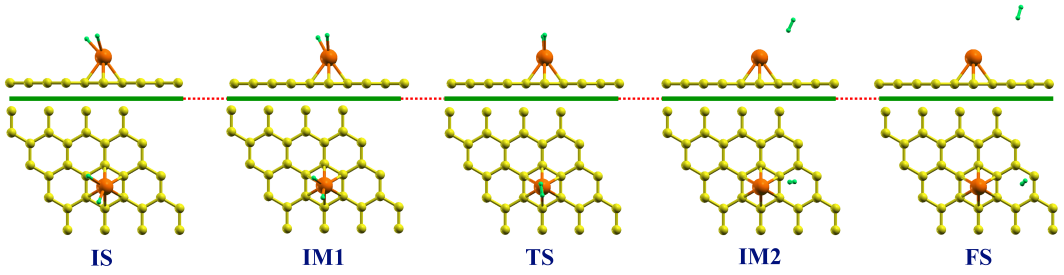

FIGURE 4.6: Generalized reaction profile of HER via VT mechanism over Ni@2D.

varies from 0.l2 eV to 1.21 eV, suggesting that overall, the VT mechanism is more preferable than the VH mechanism. The preference of VT mechanism over VH mechanism, alluding that the Ni@2D system is compatible to handle multiple H-atoms concurrently, leading to an improved catalytic performance towards HER in H-rich environment. The lowest reaction barrier is found for Ni@AlN (Al-vacancy), while some configuration like Ni@h-BN, Ni@AlC, Ni@MgO and Ni@graphene also shows relatively good catalytic activity with reaction barrier less than 0.80 eV. Overall, the lowest values of E_a are 0.12 eV and 0.21 eV for Ni@AlN and 0.28 eV

and 0.36 eV for Ni@h-BN via VT and VH mechanisms, respectively, is in exact consonance with the HER activity predicted by ΔG_H and volcano plot analysis.

4.4 Conclusion

To conclude, our DFT investigation gives a thorough insight into catalytic behaviour of Ni SACs over various class of 2D materials like graphene, AlC, AlN, h-BN, BeO and MgO (Ni@2D) towards electrocatalytic HER. To examine the stability of Ni-atoms over these substrates, we computed binding energy (E_b) of Ni-atom at all possible anchoring sites. out of all sites, we considered those configurations for which the E_b value is $<$ -3.00 eV for the H-adsorption and further analysis. Then, we proceed for the H-adsorption, also known as Volmer step and the computed adsorption energy (E_{ads}) shows the capability of Ni@2D to interact with H-atom. Further, the differential Gibbs free energy (ΔG_H) is a crucial metric to predict HER activity and according to Sabatier principle, the ΔG_H value should be close to zero for enhanced HER performance. In our case the ΔG_H value ranges from -1.57 eV to 0.49 eV, and we considered only those configurations of Ni@2D for which the $|\Delta G_H|$ is $\leq$ 0.5 eV. Consequently, out of 34 configurations at the start, we had 10 configurations of Ni@2D, which were falling in the aforementioned region. We also plotted volcano like structure between exchange current density (i_o) and ΔG_H, and as per the classical volcano theory, the top of volcano is occupied by the systems with excellent HER activity. In our case it is Ni@AlN and Ni@h-BN occupies the top, with optimum ΔG_H value of -0.06 and -0.09 eV, respectively. Also, the computed theoretical overpotential (η) which is absolute value of ΔG_H is found to be as low as 60 mV and 90 mV for Ni@AlN and Ni@h-BN, respectively. Further, we proceed for examining the complete reaction profile and minimum energy path of HER via VH and VT mechanisms over shortlisted configurations of Ni@2D. Overall, the VT mechanism is preferable over VH mechanism, with the lowest activation energy found to be 0.12 eV and 0.21 eV for Ni@AlN and 0.28 eV and 0.36 eV for Ni@h-BN via VT and VH mechanism, respectively. Thus, our investigation comprehensively discuss the catalytic activity of Ni SACs towards an electrocatalytic HER and may open the door for designing a practically operational, industrial catalyst.

Bibliography

[1] Z. Ma, L. Niu, W. Jiang *et al.* *Journal of Physics: Materials*, 4(4):042002, 2021.

[2] I. Jain. *International journal of hydrogen energy*, 34(17):7368–7378, 2009.

[3] L. Fan, Z. Tu and S. H. Chan. *Energy Reports*, 7:8421–8446, 2021.

[4] K. Mazloomi and C. Gomes. *Renewable and Sustainable Energy Reviews*, 16(5):3024–3033, 2012.

[5] L. Zhang, X. Ji, X. Ren *et al.* *Advanced Materials*, 30(28):1800191, 2018.

[6] G. D. Weatherbee and C. H. Bartholomew. *Journal of Catalysis*, 77(2):460–472, 1982.

[7] W.-H. Chen and C.-Y. Chen. *Applied Energy*, 258:114078, 2020.

[8] L. Zhou, Y. Liu, S. Liu *et al.* *Journal of Energy Chemistry*, 2023.

[9] A. Midilli, H. Kucuk, M. E. Topal *et al.* *International Journal of Hydrogen Energy*, 46(50):25385–25412, 2021.

[10] A. P. Simpson and A. E. Lutz. *International journal of hydrogen energy*, 32(18):4811–4820, 2007.

[11] M. Zeng and Y. Li. *Journal of Materials Chemistry A*, 3(29):14942–14962, 2015.

[12] A. Eftekhari. *International Journal of Hydrogen Energy*, 42(16):11053–11077, 2017.

[13] B. A. Baraiya, V. Mankad and P. K. Jha. *ChemistrySelect*, 3(37):10515–10525, 2018.

[14] J. Verma and S. Goel. *International Journal of Hydrogen Energy*, 47(92):38964–38982, 2022.

[15] L. Tian, Z. Li, M. Song *et al. Nanoscale*, 13(28):12088–12101, 2021.

[16] A. Wang, J. Li and T. Zhang. *Nature Reviews Chemistry*, 2(6):65–81, 2018.

[17] L. Liu and A. Corma. *Chemical reviews*, 118(10):4981–5079, 2018.

[18] Z. Chen, L. Chen, C. Yang *et al. Journal of Materials Chemistry A*, 7(8):3492–3515, 2019.

[19] S. K. Kaiser, Z. Chen, D. Faust Akl *et al. Chemical reviews*, 120(21):11703–11809, 2020.

[20] S. Mitchell and J. Pérez-Ramírez. *Nature communications*, 11(1):1–3, 2020.

[21] Z. Fu, B. Yang and R. Wu. *Physical review letters*, 125(15):156001, 2020.

[22] D. N. Sredojevic, M. R. Belic and Z. Sljivancanin. *The Journal of Physical Chemistry C*, 124(31):16860–16867, 2020.

[23] R. Wan, C. Wang, R. Chen *et al. International Journal of Hydrogen Energy*, 47(75):32039–32049, 2022.

[24] X.-P. Yin, H.-J. Wang, S.-F. Tang *et al. Angewandte Chemie International Edition*, 57(30):9382–9386, 2018.

[25] H. Liu, X. Peng and X. Liu. *ChemElectroChem*, 5(20):2963–2974, 2018.

[26] S. Tauster, S. Fung and R. L. Garten. *Journal of the American Chemical Society*, 100(1):170–175, 1978.

[27] J. Ekspong, E. Gracia-Espino and T. Wagberg. *The Journal of Physical Chemistry C*, 124(38):20911–20921, 2020.

[28] H. Fei, J. Dong, D. Chen *et al. Chemical Society Reviews*, 48(20):5207–5241, 2019.

[29] K. Patel, B. A. Baraiya, N. N. Som *et al. International Journal of Hydrogen Energy*, 45(37):18602–18611, 2020.

[30] Y. Bai, K. Deng and E. Kan. *RSC advances*, 5(24):18352–18358, 2015.

[31] J. Ben, X. Liu, C. Wang *et al. Advanced Materials*, 33(27):2006761, 2021.

[32] L. Liu, Y. Feng and Z. Shen. *Physical Review B*, 68(10):104102, 2003.

[33] B. Luo, Y. Yao, E. Tian *et al.* *Proceedings of the National Academy of Sciences*, 116(35):17213–17218, 2019.

[34] P. Giannozzi, S. Baroni, N. Bonini *et al.* *Journal of physics: Condensed matter*, 21(39):395502, 2009.

[35] P. Giannozzi, O. Andreussi, T. Brumme *et al.* *Journal of physics: Condensed matter*, 29(46):465901, 2017.

[36] P. E. Blöchl. *Physical review B*, 50(24):17953, 1994.

[37] G. Kresse and D. Joubert. *Physical review b*, 59(3):1758, 1999.

[38] J. P. Perdew, K. Burke and M. Ernzerhof. *Physical review letters*, 77(18):3865, 1996.

[39] S. Grimme, J. Antony, S. Ehrlich *et al.* *The Journal of chemical physics*, 132(15):154104, 2010.

[40] N. Marzari, D. Vanderbilt, A. De Vita *et al.* *Physical review letters*, 82(16):3296, 1999.

[41] H. J. Monkhorst and J. D. Pack. *Physical review B*, 13(12):5188, 1976.

[42] G. Henkelman and H. Jónsson. *The Journal of chemical physics*, 113(22):9978–9985, 2000.

[43] G. Henkelman, B. P. Uberuaga and H. Jónsson. *The Journal of chemical physics*, 113(22):9901–9904, 2000.

[44] A. Kokalj. *Journal of Molecular Graphics and Modelling*, 17(3-4):176–179, 1999.

[45] C. Zhu, Q. Shi, S. Feng *et al.* *ACS Energy Letters*, 3(7):1713–1721, 2018.

[46] T. K. Gajaria, B. Roondhe, S. D. Dabhi *et al.* *International Journal of Hydrogen Energy*, 45(44):23928–23936, 2020.

[47] A. B. Laursen, A. S. Varela, F. Dionigi *et al.* *Journal of Chemical Education*, 89(12):1595–1599, 2012.

[48] B. Conway and J. O. Bockris. *The Journal of Chemical Physics*, 26(3):532–541, 1957.

[49] J. Greeley, T. F. Jaramillo, J. Bonde *et al. Nature materials*, 5(11):909–913, 2006.

[50] J. Mou, Y. Gao, J. Wang *et al. RSC advances*, 9(21):11755–11761, 2019.

[51] F. Zhang, L. He, S. Lian *et al. The Journal of Physical Chemistry C*, 125(35):19119–19130, 2021.

[52] S. B. Pillai, B. A. Baraiya, D. Upadhyay *et al. International Journal of Hydrogen Energy*, 45(44):23900–23907, 2020.

[53] J. K. Nørskov, T. Bligaard, A. Logadottir *et al. Journal of The Electrochemical Society*, 152(3):J23, 2005.

[54] Z. W. Seh, J. Kibsgaard, C. F. Dickens *et al. Science*, 355(6321):eaad4998, 2017.

[55] R. M. Sattigeri, P. K. Jha, P. Śpiewak *et al. Applied Physics Letters*, 121(12), 2022.

[56] J. Lim, S. Back, C. Choi *et al. ChemCatChem*, 10(19):4450–4455, 2018.

[57] A. Lasia. *international journal of hydrogen energy*, 44(36):19484–19518, 2019.